JACS
JOURNAL OF THE AMERICAN CHEMICAL SOCIETY

ARTICLE

pubs.acs.org/JACS

DNA-Directed Artificial Light-Harvesting Antenna

Palash K. Dutta, Reji Varghese, Jeanette Nangreave, Su Lin, Hao Yan, and Yan Liu*

Department of Chemistry and Biochemistry and The Biodesign Institute, Arizona State University, Tempe, Arizona 85287-5601, United States

Supporting Information

ABSTRACT: Designing and constructing multichromophoric, artificial light-harvesting antennas with controlled interchromophore distances, orientations, and defined donor−acceptor ratios to facilitate efficient unidirectional energy transfer is extremely challenging. Here, we demonstrate the assembly of a series of structurally well-defined artificial light-harvesting triads based on the principles of structural DNA nanotechnology. DNA nanotechnology offers addressable scaffolds for the organization of various functional molecules with nanometer scale spatial resolution. The triads are organized by a self-assembled seven-helix DNA bundle (7HB) into cyclic arrays of three distinct chromophores, reminiscent of natural photosynthetic systems. The scaffold accommodates a primary donor array (**Py**), secondary donor array (**Cy3**) and an acceptor (**AF**) with defined interchromophore distances. Steady-state fluorescence analyses of the triads revealed an efficient, stepwise funneling of the excitation energy from the primary donor array to the acceptor core through the intermediate donor. The efficiency of excitation energy transfer and the light-harvesting ability (antenna effect) of the triads was greatly affected by the relative ratio of the primary to the intermediate donors, as well as on the interchromophore distance. Time-resolved fluorescence analyses by time-correlated single-photon counting (TCSPC) and streak camera techniques further confirmed the cascading energy transfer processes on the picosecond time scale. Our results clearly show that DNA nanoscaffolds are promising templates for the design of artificial photonic antennas with structural characteristics that are ideal for the efficient harvesting and transport of energy.

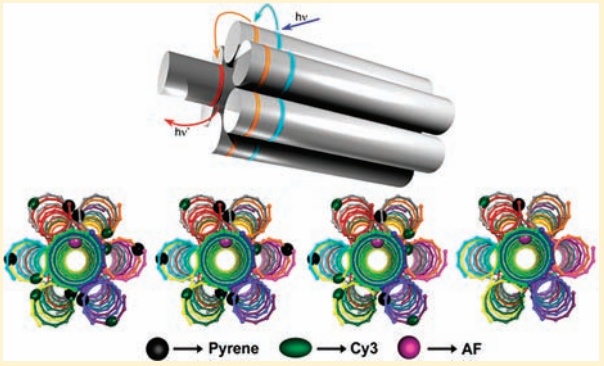

INTRODUCTION

Photosynthesis is one of the most fascinating photochemical events in nature. It is initiated by the absorption of visible light by antenna units comprised of a large number of pigment molecules, followed by funneling of the excitation energy within the antenna assembly to a reaction center where optical energy is converted to chemical energy.[1−3] The very high efficiency of natural photosynthesis is a consequence of the well-defined organization of a multitude of chromophores with distinct optical and redox properties that facilitate the efficient capture of visible light and the subsequent transfer of the excitation energy. Artificial light-harvesting systems with multiple chromophores have been found to display unidirectional energy transfer[4] and may have potential applications with the conversion of light into chemical potentials.[5] Dendrimers have been explored as covalent scaffolds for constructing arrays of chromophores that exhibit high energy transfer rates and directionality; however, it is very difficult to synthesize monodispersed dendrimers containing a large number of unique chromophores.[6] Self-assembling proteins, such as tobacco mosaic virus coat protein, have recently been demonstrated as excellent alternative scaffolds for the construction of multichromophore artificial light-harvesting antennas, offering the ability to organize several thousands of chromophores.[7−9] However, it still remains a challenge to organize multiple chromophores into arrays with well-defined interchromophore distances and control their relative orientations and the exact ratio of donors to acceptors, which are the key factors that determine the efficiency of FRET (Förster resonance energy transfer).

Structural DNA nanotechnology,[10−12] including the DNA 'origami' approach,[13] has developed to the point that fully addressable nanoarchitectures of various geometries can be easily designed and constructed. DNA nanostructures have been used as scaffolds for the directed self-assembly of many nanomaterials including nanoparticles,[14,15] quantum dots,[16,17] carbon nanotubes,[18] proteins,[19−27] and viral capsids,[28] and other functional molecules.[29] Modified phosphoramidite building blocks are commercially available and chemical modification of oligonucleotides is routinely performed with a DNA synthesizer following standard procedures. Therefore, it is relatively easy to generate chromophore-labeled oligonucleotides for subsequent incorporation into DNA nanoscaffolds, e.g., through sequence-specific hybridization. The DNA scaffolds are ideal platforms to organize arrays of multiple chromophores because of their ability to tune the distance and relative orientation between the chromophores with remarkable precision. Although there have been reports of

Received: December 21, 2010
Published: June 29, 2011

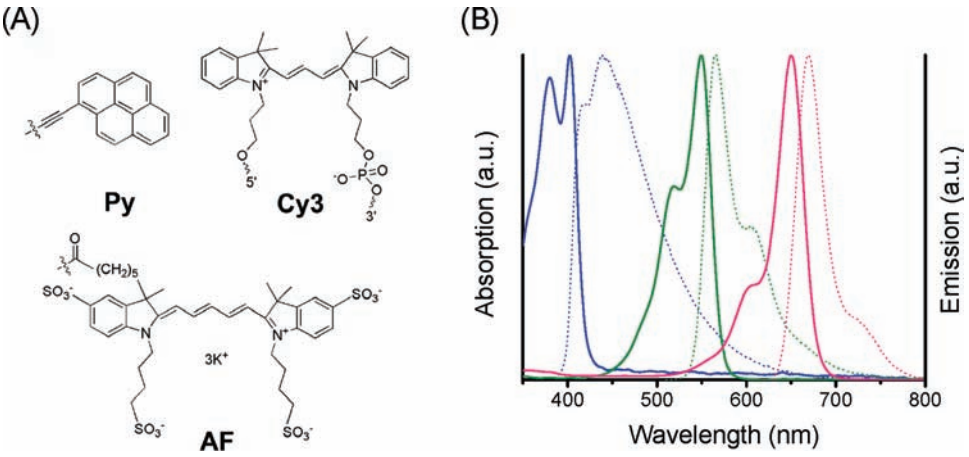

Figure 1. (A) Chemical structure of the chromophores used in this study. (B) Normalized absorption (solid line) and emission (dotted line) spectra for **Py** (blue), **Cy3** (green), and **AF** (pink) modified DNAs showing the optical spectral overlap. These spectra were obtained using the dye-labeled ssDNA hybridized to their complementary ssDNA strands (see Figure S9 (Supporting Information) for the spectral data of the dye-labeled ssDNA).

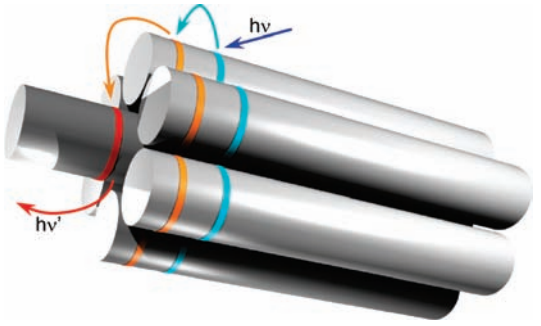

Figure 2. Schematic display of the self-assembled 7-helix bundle (7HB) nanoscaffold that contains three distinct arrays of chromophores: the primary donors, the intermediate donors, and the acceptor, represented by the cyan, orange, and red rings, respectively. Upon excitation of the primary donor array, a stepwise energy transfer cascade is observed. The distance (along the helical axes) between the dyes in adjacent arrays is 3.5 base pairs (the half base pair unit arises from the attachment of **Cy3** to the sugar−phosphate backbone between two neighboring bases) or ∼1.2 nm. The exact distances between the dyes must be calculated individually (described in greater detail in Figure S8, Supporting Information) because of the differences in the attachment method, either to the base or to the DNA backbone.

the DNA-templated organization of fluorophores into unidirectional photonic wires, it is still a challenge to engineer a large number of fluorophores into 3D geometries.[30]

Here we report the DNA-templated design and construction of a series of discrete and structurally well-defined light-harvesting systems that each consists of three different types of chromophores, organized in a manner similar to the natural light-harvesting antenna. The unidirectional, stepwise energy transfer from an array of primary donors to a single acceptor through an intermediate array of secondary donors is clearly demonstrated by steady-state and time-resolved spectral analysis. A systematic study of the effect of donor−acceptor ratios on the efficiency of FRET is also presented.

RESULTS AND DISCUSSION

The chromophores used in this study include ethynylpyrene (**Py**)[31] as the primary donor ($\lambda_{max,abs}$ = 400 nm, $\lambda_{max,em}$ = 438 nm), a cyanine-derived dye (**Cy3**) as the intermediate donor ($\lambda_{max,abs}$ = 550 nm, $\lambda_{max,em}$ = 566 nm), and Alexa Fluor 647 (**AF**)[32] as the acceptor ($\lambda_{max,abs}$ = 650 nm, $\lambda_{max,em}$ = 668 nm) (Figure 1A). The absorption and emission profiles of the chromophores show well-separated absorption and emission characteristics (Figure 1B). The spectra also reveal significant overlap between the emission of **Py**/absorption of **Cy3**, and the emission of **Cy3**/absorption of **AF**, with minimal spectral overlap between **Py** and **AF**. The spectral features of the system enable the selective excitation of distinct chromophores within the self-assembled structure, which is crucial for the examination of the cascade of energy transfer. A precise arrangement of the chromophores results in the efficient, unidirectional stepwise FRET from **Py** to **Cy3** and from **Cy3** to **AF**, with a small amount of direct FRET between **Py** and **AF**, especially when they are placed far apart. Furthermore, the three chromophores collectively absorb light throughout the entire visible spectrum (from ∼350 nm to ∼700 nm) resembling the natural light-harvesting antenna.

We used a seven-helix bundle (7HB) motif designed by Seeman and co-workers as the underlying DNA nanoscaffold.[33] The schematics shown in Figures 2 and 3 illustrate the cyclic arrangement of six helices (honeycomb cross-section) around a protruding central helix. Ring-shaped networks of multiple chromophores (arrays) with controlled interchromophore distances are coassembled with the DNA nanoscaffold by incorporating particular dye-modified oligonucleotides at selected positions. Multiple arrays of chromophores (triads) are arranged sequentially to facilitate a stepwise energy transfer cascade from the primary donor array (cyan) to the acceptor (red) through the intermediate dye array (orange, Figure 2).

The term "triad" corresponds to particular arrangements of the three chromophore arrays in the self-assembled DNA nanostructure. The four triads (**T1**−**T4**) used in this study contain dye ratios (primary donor:intermediate donor:acceptor) of 6:6:1, 6:3:1, 3:6:1, and 1:1:1, respectively. **T1**−**T4** are schematically represented in Figure 3 with the corresponding positions of the dye molecules indicated on the DNA backbone. For each of the triads in Figure 3, the primary (**Py**, black sphere) and the intermediate donors (**Cy3**, dark green oval) are distributed among the six helices in the outer ring, and the acceptor (**AF**, pink sphere) is attached to the protruding central helix (as shown in Figure 2). The two arrays of the donor chromophores

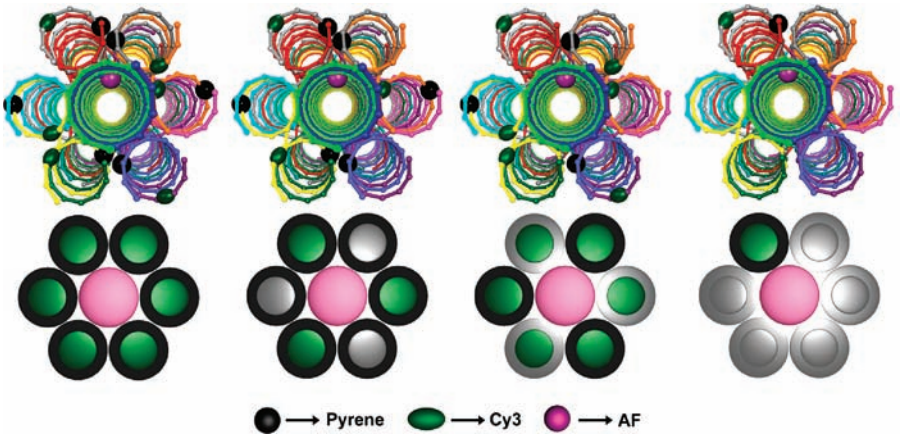

Figure 3. Schematic representation of each triad: **T1**, **T2**, **T3**, and **T4** from left to right. The black spheres, dark green ovals, and pink spheres represent **Py**, **Cy3**, and **AF**, respectively. A simplified representation of each triad is also shown below the corresponding helical schematic, where the colored circles represent the presence of the dye molecules on the DNA helices.

surround the acceptor chromophore with well-controlled inter-array distances.

In our design, the donor chromophores are attached to the DNA scaffold relatively rigidly. **Py** is incorporated into a 2′-deoxyuridine moiety through a rigid and short acetylene linker (substituting for the 5-H on the deoxyuridine base). Therefore, the aromatic ring of **Py** is expected to point toward the major groove of the corresponding DNA double helix without being fully exposed to the aqueous environment. Because of the sterics of the bulky pyrene and the nearby base pairs, the plane of the aromatic pyrene ring more likely assumes a restricted orientational distribution with respect to the DNA helix. **Cy3** is integrated within the sugar−phosphate backbone of the DNA oligonucleotide chain with a fixed orientation, linking the 5′-3′ ends of the two adjacent nucleotides.[34] As a result, its orientation is aligned with the backbone of the DNA double helix, exhibiting a well-defined angle with the helical axis. **AF** is linked to the DNA on the 5′ end through a flexible C_5 linker (see Figures S2−S6, Supporting Information). The attachment of **AF** to the DNA nanostructure is considered to be the most flexible among the three dyes. Although **AF** is highly charged with the distribution of charge spread along the periphery of the conjugation, it is still possible to stack on the end of a nearby DNA helix in a manner similar to that for cyanine dyes such as Cy3 and Cy5. When these dyes are attached to the end of double helical DNA, they interact with the DNA through base-pair stacking,[35] or may intercalate between base pairs. Although a more detailed structural analysis is required to reveal the exact conformation, static fluorescence anisotropy measurements revealed that the three dyes attached to the 7HB DNA nanostructure displayed relatively high anisotropy: Py-0.27, Cy3−0.29, and AF-0.20. These values indicate that the electric dipoles of the dyes are not allowed to freely rotate relative to the DNA nanostructure, which is consistent with the rigid attachment of the dyes to the DNA.

The Förster distances (R_0) between the dyes (Table 1) are calculated from their spectral overlap, with the assumption that the dyes behave as point dipoles with a full range of orientations (i.e., $\kappa^2 = 2/3$).[36] This assumption is not valid for our system, as we have shown that the dipoles of the dyes cannot freely rotate relative to the DNA nanostructure. However, the calculated R_0 values should provide reasonable estimates of the distances necessary for significant energy transfer interactions.

Table 1. Calculated Spectral Overlap (J) and Förster Distances (R_0) between the Dyes[a]

	J (M^{-1} cm^{-1} nm^4)	QY	κ^2	R_0 (nm)
Py−Cy3	1.235×10^{15}	0.1(**Py**)	0.66	3.63
Py−AF	5.91×10^{14}	0.1(**Py**)	0.66	3.21
Cy3−AF	1.017×10^{16}	0.23(**Cy3**)	0.66	5.93

[a] The emission and excitation spectra of the dyes used for calculating the spectral overlap (J) and the quantum yields (QY) of the two donor dyes of Py and Cy3 are measured from individual dyes labeled on the 7HB structures (100 and 010 constructs). For simplicity, the orientational factor κ^2 was assumed to be 2/3 in the calculation for R_0.

The estimated distances between the dyes in adjacent arrays and among the dyes in the same array are listed in Figures S7 and S8. For **T1** (**Py**:**Cy3**:**AF** = 6:6:1), the shortest distances between the **Py** and **Cy3** dye molecules are calculated to be in the range of 2.1−2.7 nm, based on the underlying DNA nanostructure and the rigidity of the dye attachments. This distance range is significantly smaller than the calculated Förster distance for these two dyes (3.63 nm), and as a result efficient FRET can occur between neighboring **Py** and **Cy3** pairs. The distance between the single **AF** acceptor and the six **Cy3** dyes in the adjacent array ranges from ∼1.8 nm (shortest) to ∼4.5 nm (longest), all of which are smaller than the Förster distance between **Cy3** and **AF** (∼5.93 nm); thus, an efficient FRET between these dyes is also expected. The two shortest distances between the six **Py** dyes and the single **AF** acceptor are 2.4 and 2.6 nm, which are smaller than the calculated Förster distance between these two dyes. However, the FRET efficiency between **Py** and **AF** is expected to be lower than between the other pairs of dyes. A comparison of the Förster distances suggests that the most efficient energy transfer pathways in each triad are between the neighboring **Py**/**Cy3** and **Cy3**/**AF** pairs.

The **Py**- and **Cy3**-modified ssDNAs were created with a DNA synthesizer (ABI, 394 DNA/RNA Synthesizer, Applied Biosystems) using commercially available phosphoramidites (Glen Research), purified by reverse phase HPLC (Agilent 1200, equipped with both UV photodiode detector and automated fraction collector), and characterized using matrix-assisted laser desorption ionization time-of-flight (MALDI-TOF) mass spectroscopy (Applied

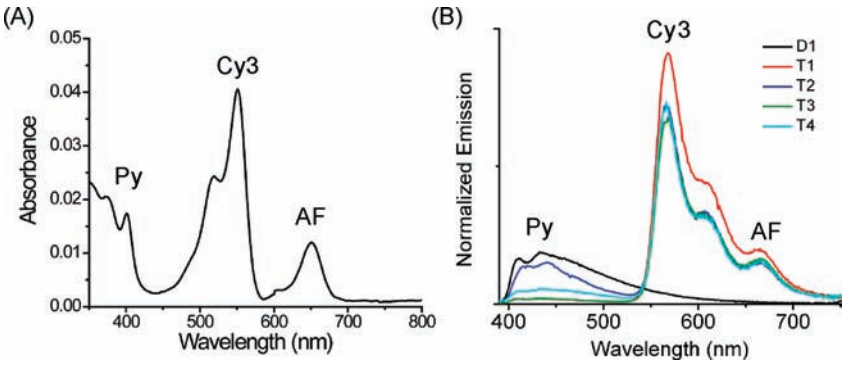

Figure 4. (A) Absorption spectrum of **T1** (additional absorption spectra are shown in Figure S10). (B) Normalized emission spectra of **D1** and **T1**−**T4**, all with excitation at 380 nm. For all samples, the emission spectra were corrected by the PMT detector spectral response file within the instrument software, and the normalization was done by dividing the emission spectra by the absorption value of each individual sample at 380 nm. The original raw absorption and emission data are shown in Figures S10 and S11.

Biosystem Voyager System 4320) (see Supporting Information for sequences and additional characterization details). **AF**-modified and all other unmodified DNAs were purchased from Integrated DNA Technologies (www.idtdna.com) and purified by denaturing polyacrylamide gel electrophoresis (PAGE). The DNA nanoscaffold templated triads were constructed by mixing equimolar amounts of the appropriate DNA strands in 1 × TAE buffer containing ∼63.4 mM of Mg^{2+} and annealed from 90 °C to room temperature over 12 h. The formation of the desired 7HB structures was confirmed by nondenaturing polyacrylamide gel electrophoresis (Native PAGE, 5%), and the bands corresponding to the assembled structures were excised and extracted from the gels. The purified structures were again analyzed by Native PAGE and visualized with a fluorescence gel imager (Typhoon Trio multifunction imager, Amersham Biosciences), as shown in Figure S1. For all four cases, the designed triads (**T1**−**T4**) migrated as a single, discrete band containing all the dye molecules as expected. The relative intensities of the bands in the fluorescence gel images also reflect the various ratios of dye molecules in particular structures.

A UV−vis absorption spectrum of each purified structure was collected by a Jasco V-670 spectrophotometer (shown in Figure 4A, and Figure S10, Supporting Information). The buffer solution was used to collect a background signal. On the basis of the extinction coefficients of the dyes, the concentration of each sample was found to be in the range of 50−80 nM. Each triad absorbs throughout the entire visible spectrum (350−700 nm) with distinct, well separated peaks at 400, 550, and 650 nm, characteristic of the **Py**, **Cy3**, and **AF** chromophores, respectively. The multidye absorption spectrum contains an essentially linear combination of the individual spectra, confirming that there are no ground-state interactions between the chromophores in the self-assembled structures. The formation of intramolecular excimers was not observed, even for those cases in which pairs of **Py** or **Cy3** dyes within the same array are spaced very closely (∼0.8 nm). The structures that contain particular numbers of chromophores are easily distinguished from the ratios of the characteristic absorbance peaks. The FRET process for each triad was investigated in detail using both steady-state and time-resolved fluorescence spectroscopy techniques. The fluorescence spectrum of a control structure (**D1**) that resembles **T1** but contains an array of six **Py** only (with no **Cy3** nor **AF**) exhibited emission features characteristic of a monomeric **Py** (Figure 4B, black trace).

When **T1** (with dye ratio of 6:6:1) is excited at 380 nm (the wavelength of **Py** absorption), a drastic quenching of **Py** emission at 438 nm compared to that of **D1**, and strong emission peaks at 566 and 668 nm that are characteristic of **Cy3** and **AF**, respectively, are observed (Figure 4B, red trace). From this data, the FRET efficiency, calculated from the decrease in **Py** emission, is estimated to be ∼90%. The observed emission from **AF** upon photoexcitation of **Py** is most likely due to the stepwise energy transfer from the **Py** array to **AF** through the intermediate **Cy3** array. This is confirmed by the analysis of a dyad control sample (**D2**) that is structurally similar to **T1**, containing six **Py** and one **AF** but lacking the intermediate **Cy3** array. **D2** exhibited a very weak emission peak at 668 nm, with the same 380 nm excitation (shown in Figure S11B, Supporting Information). Although the direct energy transfer from **Py** to **AF** cannot be completely ignored, its occurrence is significantly reduced in the presence of the **Cy3** array. This is primarily because **Cy3** has larger spectral overlap with both **Py** and **AF** and is positioned more closely to **Py** and **AF** than they are to each other.

The efficiency of energy transfer is strongly influenced by the ratio of **Py** to **Cy3**. For example, **T1**, with a **Py**:**Cy3** ratio of 6:6 (=1:1), exhibits a remarkable FRET efficiency up to ∼90%. In the case of **T2**, with a **Py**:**Cy3** ratio of 6:3 (=2:1), the FRET efficiency is drastically reduced to ∼30%. This may be because of the decrease in the number of **Cy3** in this triad; in the moments after excitation, only half of the excited **Py** can find a proximal **Cy3** to relay the energy to, while the other half of **Py** either have to relay the energy to a more distant **Cy3** via a slower energy transfer or relax back to the ground state by fluorescence emission or nonradiative pathways. However, for **T3**, reversing the **Py**:**Cy3** ratio to 3:6 (=1:2) restores the FRET efficiency to ∼90%, similar to the **T1** triad. This implies that the FRET efficiency reaches a maximum value when the number of intermediate donor **Cy3** molecules is maximized. Reducing the number of primary donor **Py** molecules does not have any considerable effects on the energy transfer efficiency, and only reduces the initial amount of light absorbed. It is important to note that the FRET efficiency in **T4** (**Py**:**Cy3**:**AF** = 1:1:1) is ∼70%, lower than that for **T1**, even though both triads have the same **Py**:**Cy3** ratio of 1:1 and the same distance (shortest) between **Py** and **Cy3**. This difference in the FRET efficiency indicates that the presence of multiple **Py** and **Cy3** pairs in **T1** provides several energy transfer pathways. Therefore, **T1** exhibits energy transfer efficiencies significantly higher than those of **T4**, which only contains a single pathway.

It is important to acknowledge that the expected FRET efficiencies (based on the Förster distances) are larger than the measured values, possibly because of orientation effects. The allowed angles and relative orientations between the dipole moments of the chromophores may not be optimized for the most efficient energy transfer because of the relatively rigid attachment of the dyes to the DNA nanostructures. The number of possible orientations of the dyes is limited by their individual conformation with respect to the helical axis of the DNA and by their position within the DNA helix. In addition, because of the antiparallel alignment of the complementary strands within each DNA helix, two dyes labeled on the same DNA strand may assume a 180° relative orientation when they are separated by a crossover point. These effects can dramatically decrease the value of κ^2 (the orientation effect), thus reducing the observed FRET efficiency.

In addition to evaluating the FRET efficiency of each energy transfer step, the light-harvesting ability of each triad is determined by evaluating the so-called "antenna" effect,[7a] which is defined as the ratio of the fluorescence intensity of the acceptor upon excitation of the donor to that of the direct excitation of the acceptor. The antenna effect indicates an overall increase or decrease in the *acceptor emission* resulting from a change in the *donor*, whereas the efficiency of energy transfer specifies the increase or decrease in *donor emission* with a change in the *acceptor*. The overall antenna effect (AE1) is calculated using the following equation: AE1 = $I_{AF,380nm}/I_{AF,620nm}$, where $I_{AF,380\ nm}$ and $I_{AF,620\ nm}$ are the fluorescence intensities of **AF** upon excitation of the primary donor (**Py**) at 380 nm and the direct excitation of **AF** at 620 nm. The antenna effect for the second step (AE2) is calculated according to the following equation: AE2 = $I_{AF,500nm}/I_{AF,620nm}$, that compares the fluorescence intensity of AF upon excitation of the intermediate donor **Cy3** at 500 nm to the direct excitation of **AF**.

The overall antenna effect for **T1** is ~85%, indicating that the emission of the **AF** acceptor, after indirect excitation through stepwise FRET energy transfer from the **Py** donors, is only slightly lower than the emission when the acceptor is directly excited. This result demonstrates that the light-harvesting capability of our system is quite efficient. The antenna effect was negligible for a control construct which contained only the acceptor without the primary and intermediate donor arrays, because 380 nm light is not efficiently absorbed by the acceptor.

The antenna effects for triads **T2**, **T3**, and **T4** were analyzed to determine the effect of the number of donors on the light-harvesting ability. **T2** and **T3** with **Py**:**Cy3**:**AF** ratios of 6:3:1 and 3:6:1 demonstrate comparable antenna effects of ~43% and ~47%, respectively, which is about half of the antenna effect of **T1**. **T2**, with six primary donors, initially absorbs the same amount of light as **T1**; however, **T2** only has three intermediate donors to relay the energy to the final acceptor (compared to six intermediated donors in **T1**), and the result is a decrease in the antenna effect. While **T3** has six intermediate donors to transfer the energy to **AF**, the initial amount of light absorbed by the three **Py** chromophores is approximately half that of **T1**, producing a reduction similar to the antenna effect for **T2**. The antenna effect is only ~16% for **T4**, which has a single **Py** and **Cy3** donor molecule. Although the relative number of **Py** to **Cy3** is the same for **T1** and **T4**, the initial absorption of energy by a single **Py** molecule in **T4** results in a significant decrease in the antenna effect.

By definition, the antenna effect is an empirical measure of the light-harvesting efficiency of a system. It is proportional to the product of the efficiencies of each energy transfer step, to the ratio of the extinction coefficients of the donor and the acceptor at their excitation wavelengths and to the ratio of the number of donor to acceptor dyes (i.e., the ratio of the excitation photons absorbed at the different wavelengths). The greater the number of primary donors to absorb light in the first step of the energy cascade, the greater the energy available for the downstream transfer of energy; in addition, the higher the efficiency of the energy transfer between dyes, the more light that will be emitted by the final acceptor of the relay. **T1** has six **Py** and six **Cy3**; **T2** has six **Py** and three **Cy3**; **T3** has three **Py** and six **Cy3**; and **T4** has one **Py** and one **Cy3**, and although the initial energy gain by **T1** and **T2** are the same, the intermediate transfer of energy through **Cy3** is not equal for the two triads. Therefore, we can predict the overall antenna effect will exhibit a trend of **T1** > **T2** ≈ **T3** > **T4**, with an approximate ratio of 6:3:3:1. This trend was experimentally confirmed (Table 2).

Table 2. The Measured FRET Efficiency and Antenna Effect for Each Triad, Where the FRET Efficiency Is Calculated by the Quenching of Py Emission Compared to the D1 Sample[a]

system	FRET efficiency (%)	antenna effect 1 (%)	antenna effect 2 (%)
T1 (6:6:1)	90	85	93
T2 (6:3:1)	30	43	39
T3 (3:6:1)	90	47	89
T4 (1:1:1)	70	16	16

[a] Antenna effects 1 and 2 are obtained by comparing the emission of **AF** by excitation at **Py** or **Cy3** to the emission of **AF** by direct excitation.

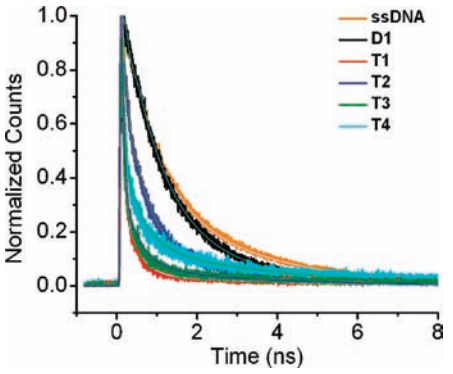

Figure 5. Fluorescence decay profile of ssDNA (5′-ATTATA**Py**A-TAGCGTCGTGCGACTGGCA-TGTGATAC-3′), **D1**, and **T1**−**T4** monitored at 460 nm (λ_{ex} = 370 nm).

The antenna effect for the second step of the energy transfer cascade can be evaluated by the direct excitation (500 nm) of the secondary donor (**Cy3**) (Table 2). The predicted trend for antenna effect 2 (**T1** ≈ **T3** > **T2** > **T4**) is based on the number of **Cy3** chromophores in each triad, which exhibit a ratio of 6:6:3:1. The experimental results are in reasonable agreement with the predicted values. Overall, the results indicate that the excitation energy can be efficiently funneled in a stepwise manner to the acceptor core by peripheral donor excitation.

Detailed time-resolved fluorescence analyses were performed on each triad to elucidate the kinetics and dynamics of the cascading FRET processes. First, time-correlated single-photon counting (TCSPC) was used for fluorescence decay analysis (Figure 5). The decay analysis of the individual **Py**, **Cy3**, and **AF**

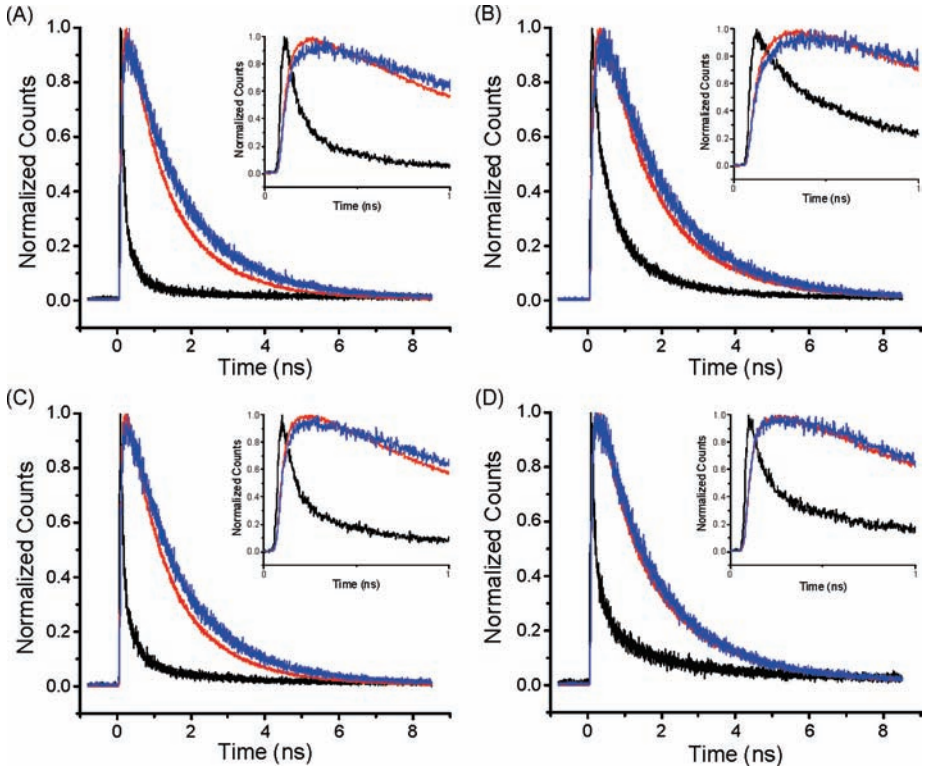

Figure 6. Time-resolved emission of **T1** (A), **T2** (B), **T3** (C), and **T4** (D) monitored at 460 nm (**Py** decay, black), 560 nm (**Cy3** decay, red), and 660 nm (**AF** decay, blue).

constructs revealed biexponential decay profiles with lifetimes of 0.35 and 3.2 ns for **Py**, 0.45 and 2.1 ns for **Cy3**, and 0.34 and 1.3 ns for **AF** (see Figure S20, Supporting Information). Figure 5 contains the decay profiles of **Py** in **D1** and **T1**−**T4**, monitored at 460 nm (using λ_{ex} = 370 nm). The profiles clearly show that the decay of **Py** becomes faster in the presence of **Cy3** and **AF** as the number of **Cy3** molecules is increased, following the trend revealed by the steady-state FRET efficiency measurements (**T1** ≈ **T3** > **T4** > **T2**). The significant acceleration of the decay dynamics of the **Py** donor in the presence of the acceptors provides clear evidence of FRET.

Further evidence of a stepwise energy transfer process is provided by the rise in the emission of **Cy3** and **AF**, monitored at 560 and 660 nm, respectively, upon excitation of **Py** at 370 nm (Figure 6). At the initial time scale (∼10 ps to ∼300 ps) the observed rise component for **Cy3** and **AF** in **T1**−**T4** coincides with the decay of **Py**, representing an increasing excited-state population of both chromophores through energy transfer from the photoexcitation of **Py**. In addition, the rise and decay of **AF** is slower than that for **Cy3** in all four cases, indicating that **AF** is involved in the final step of the stepwise energy transfer relay. For **T4**, the rise and decay of **AF** follows that of **Cy3** very closely, probably because of the particular arrangement of the dyes; the distance between **Cy3** and **AF** is similar to the distance between **Py** and **AF** with the potential for one step energy transfer from **Py** to **Cy3** and **Py** to **AF**.

The TCSPC instrument response time is on the order of ∼40 ps, and thus very short lifetimes cannot be obtained reliably. To improve the temporal resolution, a streak camera was utilized. Emission decay data from a spectral range of 450 to 680 nm, with excitation at 370 nm, was obtained for each triad sample. The instrument simultaneously provided high temporal resolution (∼2 ps) and high spectral resolution (∼5 nm). The 3D data for a typical sample is shown in Figure S14, Supporting Information, and additional decay profiles at various wavelengths are shown in Figures S16−S19, Supporting Information. Global lifetime analyses was performed using the same set of lifetimes for the decay at different wavelengths; this determines the spectral dependence of the decay amplitudes associated with each lifetime, also known as the decay-associated spectra (DAS) (shown in Figure 7). DAS offers better insight into the mechanisms of multistep energy transfer processes than emission decays monitored at a single wavelength. **T4** can be adequately described by three lifetime components, while the other three samples **T1**−**T3** require an additional component.

The lifetimes for the **T4** fluorescence decay profile (with a dye ratio of 1:1:1) are 40 ps, 0.43 ns, and 2.4 ns. The corresponding DAS spectrum (Figure 7) for the component with the shortest lifetime (40 ps) shows a positive amplitude in the **Py** emission region (450−540 nm) and a negative amplitude in the **Cy3** emission region (540−650 nm). These spectral features indicate that the 40 ps lifetime component corresponds to the decay of the **Py** excited-state population with the simultaneous buildup of the **Cy3** excited-state population, resulting from the energy transfer from **Py** to **Cy3** that occurs within this short lifetime. The 40 ps lifetime data also shows small negative amplitude in the **AF** spectral range, indicating that the population buildup of the excited state of **AF** may occur in a similar time scale as **Cy3**. This may suggest a very fast energy transfer rate from **Cy3** to **AF**, possibly with a small amount of direct energy transfer from **Py** to **AF** (Figure S23, Supporting Information). The DAS spectra of the components for the 0.43 and 2.4 ns lifetimes contain one

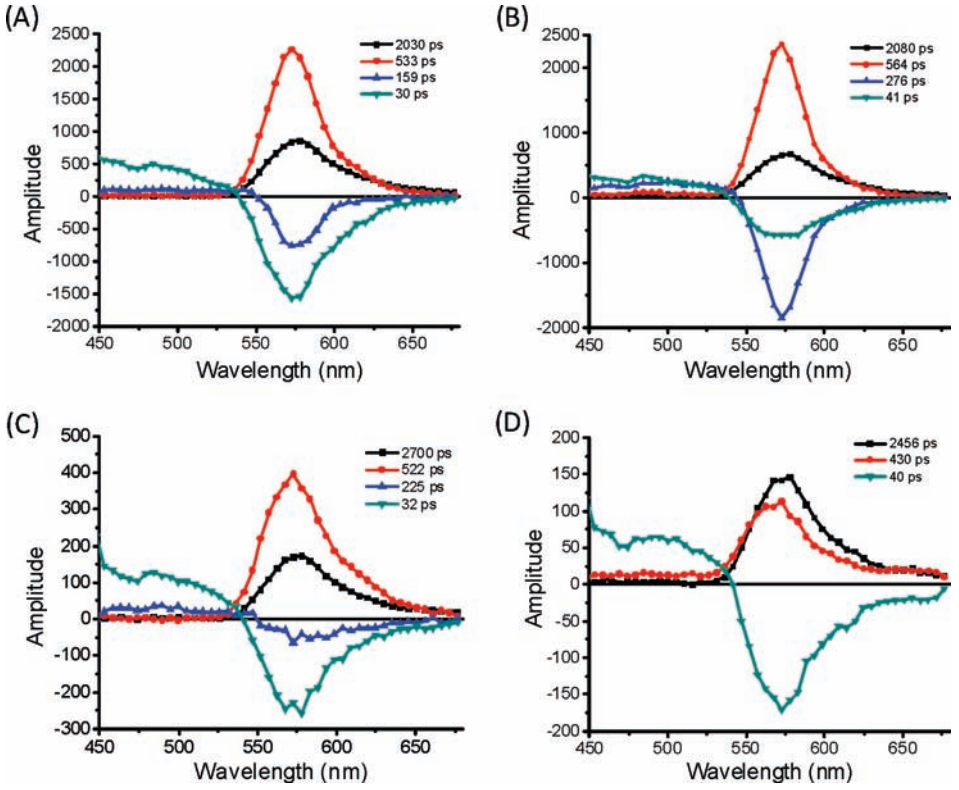

Figure 7. DAS of (A) **T1** (6:6:1), (B) **T2** (6:3:1), (C) **T3** (3:6:1), and (D) **T4** (1:1:1), where the numbers in the parentheses indicate the ratio of the three dyes in each structure.

main, intense positive band in the **Cy3** emission region, which can be attributed to the decay of the excited-state population of **Cy3** resulting from the energy transfer from **Cy3** to **AF** and the decay of **Cy3** to its ground state. However, the small positive (nonzero) amplitudes at 450 and 660 nm for these two components also indicate minor contributions from **Py** and **AF** decays in the longer lifetime scale, consistent with the results obtained by the TCSPC.

The fluorescence decay profile for **T3** (with dye ratio of 3:6:1) exhibits a four-exponential decay with lifetimes of 32 ps, 225 ps, 522 ps, and 2.7 ns. The two shortest lifetimes display positive amplitudes in the **Py** spectral region and negative amplitudes in the **Cy3** and **AF** spectral region, which represent the **Cy3** population buildup and the simultaneous decay of **Py**; the two longer lifetimes exhibit positive amplitudes in the **Cy3** and **AF** spectral region, representing the decay of the two acceptor dyes. The occurrence of two short lifetime components also indicates that both the short (∼2.1 nm) and long (∼3.5 nm) distance energy transfer processes between **Py** and **Cy3** occur in **T3**, corresponding to the two lifetimes, 32 and 225 ps, respectively. Of the two shorter lifetime components, the shortest component has a far more negative amplitude than the second shortest component, which indicates that the short-range pathway dominates in the energy transfer process. This is probably because of the smaller ratio of **Py** to **Cy3** in this sample (3:6), i.e., although every excited **Py** has at least two **Cy3** to transfer energy to, the **Cy3** that is the closest to **Py** likely wins the kinetic competition.

Triads **T1** and **T2**, with a larger number of primary donor molecules, also display four lifetimes: 30 ps, 159 ps, 533 ps, and 2 ns for **T1**, and 41 ps, 276 ps, 564 ps, and 2.1 ns for **T2**. Similar to **T3**, the two shortest lifetime components in the DAS spectra for **T1** and **T2** both exhibit positive amplitudes in the **Py** emission region due to the excited-state decay of **Py**, and negative amplitudes in the **Cy3** and **AF** emission region due to the simultaneous population increase of the excited state of **Cy3** and **AF**.

The long-range energy transfer pathway (with lifetimes of 160−270 ps) has a slightly more important role in **T1** (**Py**:**Cy3** = 6:6, Figure 7A) than in **T3** (**Py**:**Cy3** = 3:6, Figure 7C). It is expected that as more **Py** molecules are available for excitation, the probability of the long-range energy transfer process increases. However, in **T2** (**Py**:**Cy3** = 6:3) the longer range energy transfer component shows a larger amplitude than the shortest lifetime component (Figure 7B). One possible explanation for this is that every **Py** in **T2** has the same probability of being excited; however, only half of the excited chromophores can find a nearby **Cy3** to accept energy, while the other half would have to transfer energy via the longer distance pathway. At the same time, the **Py** in **T2** that have nearby **Cy3** also have a probability of transferring the energy through the longer distance pathway, as seen in the case of **T1** and **T3**.

It should be noted that the DAS associated with the ∼500 ps lifetime, which should reflect the energy transfer from **Cy3** to **AF**, does not exhibit the expected signature shape as seen in the ∼40 ps DAS. It is likely that the negative amplitude in the **AF** spectral region is superimposed on the positive signal from **Cy3** emission with the same time constant. However, comparison of the ∼500 ps DAS with the ∼2 ns DAS reveals an obvious amplitude increase in the **AF** emission in the 2 ns DAS (Figure S24, Supporting Information). This confirms that the relative excited-state population of **AF** to **Cy3** has increased in the later time and provides evidence that the energy transfer from **Cy3** to **AF** occurs within 500 ps.

CONCLUSION

We have employed DNA nanotechnology to create a structurally well-defined, DNA templated, artificial light-harvesting antenna. Three distinct chromophore arrays were arranged into several triad configurations with precise interchromophore distance and well-defined donor−acceptor ratios. Steady-state and time-resolved fluorescence analyses revealed that efficient, stepwise FRET from a primary donor array to an acceptor through an intermediate donor array occurs upon excitation of the primary donor. Although multiple energy transfer pathways are possible in each multidye array, unidirectional energy transfer to the final acceptor was always observed. In addition, the relative donor−acceptor ratio had a profound effect on the efficiency of energy transfer and the antenna effect.

This study undoubtedly demonstrates that DNA-based nanoscaffolds are excellent platforms to organize arrays of chromophores with precise control of each structural element and provide the flexibility necessary to test several factors governing the antenna effect, such as the molar ratio of the dyes, the ratio of the extinction coefficients of the donor and acceptor, the quantum yields, and the spectral overlap. It may ultimately provide essential guidelines for the future design of artificial light-harvesting systems. For example, for an efficient light-harvesting system, the antenna dyes should cover a broad absorption range, have high extinction coefficients, high quantum yields, and broad emission spectra. The dyes used here are far from optimized to achieve the best light-harvesting efficiency. Other blue absorbing dyes with higher extinction coefficients and higher quantum yields may be considered in the future, and more complex design could be employed to further improve the light-harvesting ability and energy transfer efficiency.

ASSOCIATED CONTENT

Supporting Information. Methods, calculation of FRET efficiency, gel electrophoresis, DNA sequences, additional spectral data, and DNA synthesis and modification characterization. This material is available free of charge via the Internet at http://pubs.acs.org.

AUTHOR INFORMATION

Corresponding Author
yan_liu@asu.edu.

ACKNOWLEDGMENT

This research was partly supported by grants from the NSF, ONR, ARO, and DOE to Y.L.; Y.L. and H.Y. were supported as part of the Center for Bio-Inspired Solar Fuel Production, an Energy Frontier Research Center funded by the U.S. Department of Energy, Office of Science, Office of Basic Energy.

REFERENCES

(1) (a) *Photosynthetic Light Harvesting Systems*; Scheer, H.; Schneider, S., Eds.;Walter de Gruyter: Berlin, 1988. (b) *Energy Harvesting Materials*; Andrews, D. L., Ed.; World Scientific: Singapore, 2005.

(2) Hu, X.; Damjanović, A.; Ritz, C.; Schulten, K. *Proc. Natl. Acad. Sci. U.S.A.* **1998**, *95*, 5935.

(3) McDermott, G.; Prince, S. M.; Freer, A. A.; Hawthornthwaite-Lawless, A. M.; Papiz, M. Z.; Cogdell, R. J.; Isaacs, N. W. *Nature* **1995**, *374*, 517.

(4) (a) Schenning, A. P. H. J.; Benneker, F. B. G.; Geurts, H. P. M.; Liu, X. Y.; Nolte, R. J. M. *J. Am. Chem. Soc.* **1996**, *118*, 8549. (b) Jullien, L.; Canceill, J.; Valeur, B.; Bardez, E.; Lefèvre, J.-P.; Lehn, J.-M.; Marchi-Artzner, V.; Pansu, R. *J. Am. Chem. Soc.* **1996**, *118*, 5432. (c) Würthner, F.; Sautter, A. *Org. Biomol. Chem.* **2003**, *1*, 240. (d) Choi, M.-S.; Yamazaki, T.; Yamazaki, I.; Aida, T. *Angew. Chem., Int. Ed.* **2004**, *43*, 150. (e) Sautter, A.; Kaletaş, K. K.; Schmid, D. G.; Dobrawa, R.; Zimine, M.; Jung, G.; Stokkum, I. H. M.; De Cola, L.; Williams, R. M.; Würthner, F. *J. Am. Chem. Soc.* **2005**, *127*, 6719. (f) Nakamura, Y.; Aratani, N.; Osuka, A. *Chem. Soc. Rev.* **2007**, *36*, 831. (g) Aratani, N.; Kim, D.; Osuka, A. *Acc. Chem. Res.* **2009**, *42*, 1922. (h) Terazono, Y.; Kodis, G.; Liddell, P. A.; Garg, V.; Moore, T. A.; Moore, A. L.; Gust, D. *J. Phys. Chem. B* **2009**, *113*, 7147. (i) Boeneman, K.; Deschamps, J. R.; Buckhout-White, S.; Prasuhn, D. E.; Blanco-Canosa, J. B.; Dawson, P. E.; Stewart, M. H.; Susumu, K.; Goldman, E. R.; Ancona, M.; Medintz, I. L. *ACS Nano* **2010**, *4*, 7253. (j) Boeneman, K.; Prasuhn, D. E.; Blanco-Canosa, J. B.; Dawson, P. E.; Melinger, J. S.; Ancona, M.; Stewart, M. H.; Susumu, K.; Huston, A.; Medintz, I. L. *J. Am. Chem. Soc.* **2010**, *132*, 18177. (k) Hannestad, J. K.; Sandin, P.; Albinsson, B. *J. Am. Chem. Soc.* **2008**, *130*, 15889.

(5) (a) Gust, D.; Moore, T. A.; Moore, A. L. *Acc. Chem. Res.* **1993**, *26*, 198. (b) Gust, D.; Moore, T. A.; Moore, A. L. *Acc. Chem. Res.* **2001**, *34*, 40.

(6) (a) Schenning, A. P. H. J.; Peeters, E.; Meijer, E. W. *J. Am. Chem. Soc.* **2000**, *122*, 4489. (b) Adronov, A.; Fréchet, J. M. J. *Chem. Commun.* **2000**, 1701. (c) Weil, T.; Reuther, E.; Müllen, K. *Angew. Chem., Int. Ed.* **2002**, *41*, 1900. (d) Choi, M.-S.; Aida, T.; Yamazaki, T.; Yamazaki, I. *Chem.—Eur. J.* **2002**, *8*, 2667. (e) Hahn, U.; Gorka, M.; Vögtle, F.; Vicinelli, V.; Ceroni, P.; Maestri, M.; Balzani, V. *Angew. Chem., Int. Ed.* **2002**, *41*, 3595. (f) Balzani, V.; Ceroni, P.; Maestri, M.; Vicinelli, V. *Curr. Opin. Chem. Biol.* **2003**, *7*, 657. (g) Imahori, H. J. *Phys. Chem. B* **2004**, *108*, 6130. (h) Cotlet, M.; Vosch, T.; Habuchi, S.; Weil, T.; Müllen, K.; Hofkens, J.; De Schryver, F. *J. Am. Chem. Soc.* **2005**, *127*, 9760.

(7) (a) Miller, R. A.; Presley, A. D.; Francis, M. B. *J. Am. Chem. Soc.* **2007**, *129*, 3104. (b) Ma, Y.-Z.; Miller, R. A.; Fleming, G. R.; Francis, M. B. *J. Phys. Chem. B* **2008**, *112*, 6887. (c) Miller, R. A.; Stephanopoulos, N.; McFarland, J. M.; Rosko, A. S.; Geissler, P. L.; Francis, M. B. *J. Am. Chem. Soc.* **2010**, *132*, 6068.

(8) Endo, M.; Fujitsuka, M.; Majima, T. *Chem.—Eur. J.* **2007**, *13*, 8660.

(9) (a) Scolaro, L. M.; Castriciano, M. A.; Romeo, A.; Micali, N.; Angelini, N.; Lo Passo, C.; Felici, F. *J. Am. Chem. Soc.* **2006**, *128*, 7446. (b) Nam, Y. S.; Shin, T.; Park, H.; Magyar, A. P.; Choi, K.; Fantner, G.; Nelson, K. A.; Belcher, A. M. *J. Am. Chem. Soc.* **2010**, *132*, 1462.

(10) (a) Seeman, N. C. *J. Theor. Biol.* **1982**, *99*, 237. (b) Seeman, N. C. *Mol. Biotechnol.* **2007**, *37*, 246. (c) Seeman, N. C. *Nano Lett.* **2010**, *10*, 1971.

(11) Lin, C.; Liu, Y.; Rinker, S.; Yan, H. *ChemPhysChem* **2006**, *7*, 1641.

(12) Aldaye, F. A.; Palmer, A. L.; Sleiman, H. F. *Science* **2008**, *321*, 1795.

(13) Rothemund, P. W. K. *Nature* **2006**, *440*, 297.

(14) (a) Zhang, J.; Liu, Y.; Ke, Y.; Yan, H. *Nano Lett.* **2006**, *6*, 248. (b) Sharma, J.; Chhabra, R.; Liu, Y.; Ke, Y.; Yan, H. *Angew. Chem., Int. Ed.* **2006**, *45*, 730. (c) Sharma, J.; Chhabra, R.; Cheng, A.; Brownell, J.; Liu, Y.; Yan, H. *Science* **2009**, *323*, 112. (d) Stearns, L. A.; Chhabra, R.; Sharma, J.; Liu, Y.; Petuskey, W. T.; Yan, H.; Chaput, J. C. *Angew. Chem., Int. Ed.* **2009**, *48*, 8494. (e) Ding, B.; Deng, Z.; Yan, H.; Cabrini, S.; Zuckermann, R. N.; Bokor, J. *J. Am. Chem. Soc.* **2010**, *132*, 3248. (f) Pal, S.; Deng, Z.; Ding, B.; Yan, H.; Liu, Y. *Angew. Chem., Int. Ed.* **2010**, *49*, 2700. (g) Hung, A. M.; Micheel, C. M.; Bozano, L. D.; Osterbur, L. W.; Wallraff, G. M.; Cha, J. N. *Nat. Nanotechnol.* **2010**, *5*, 121. (h) Kuzuya, A.; Koshi, N.; Kimura, M.; Numajiri, K.; Yamazaki, T.; Ohnishi, T.; Okada, F.; Komiyama, M. *Small* **2010**, *6*, 2664.

(15) (a) Pinto, Y. Y.; Le, J. D.; Seeman, N. C.; Musier-Forsyth, K.; Taton, T. A.; Kiehl, R. A. *Nano Lett.* **2005**, *5*, 2399. (b) Zheng, J.; Constantinou, P. E.; Micheel, C.; Alivisatos, A. P.; Kiehl, R. A.; Seeman, N. C. *Nano Lett.* **2006**, *6*, 1502.

(16) Sharma, J.; Ke, Y.; Lin, C.; Chhabra, R.; Wang, Q.; Nangreave, J.; Liu, Y.; Yan, H. *Angew. Chem., Int. Ed.* **2008**, *47*, 5157.

(17) Bui, H.; Onodera, C.; Kidwell, C.; Tan, Y.; Graugnard, E.; Kuang, W.; Lee, J.; Knowlton, W. B.; Yurke, B.; Hughes, W. L. *Nano Lett.* **2010**, *10*, 3367.
(18) Maune, H. T.; Han, S.-p.; Barish, R. D.; Bockrath, M.; Goddard, W. A., III; Rothemund, P. W. K.; Winfree, E. *Nat. Nanotechnol.* **2010**, *5*, 61.
(19) (a) Yan, H.; Park, S. H.; Finkelstein, G.; Reif, J. H.; LaBean, T. H. *Science* **2003**, *30*, 1882. (b) Li, H.; Park, S. H.; Reif, J. H.; LaBean, T. H.; Yan, H. *J. Am. Chem. Soc.* **2004**, *126*, 418. (c) Park, S. H.; Yin, P.; Liu, Y.; Reif, J. H.; LaBean, T. H.; Yan, H. *Nano Lett.* **2005**, *5*, 729. (d) Park, S. H.; Pistol, C.; Ahn, S. J.; Reif, J. H.; Lebeck, A. R.; Dwyer, C.; LaBean, T. H. *Angew. Chem., Int. Ed.* **2006**, *45*, 735.
(20) (a) Liu, Y.; Lin, C.; Li, H.; Yan, H. *Angew. Chem., Int. Ed.* **2005**, *44*, 4333. (b) Williams, B. A. R.; Lund, K.; Liu, Y.; Yan, H.; Chaput, J. C. *Angew. Chem., Int. Ed.* **2007**, *46*, 3051. (c) Chhabra, R.; Sharma, J.; Ke, Y.; Liu, Y.; Rinker, S.; Lindsay, S.; Yan, H. *J. Am. Chem. Soc.* **2007**, *129*, 10304. (d) Rinker, S.; Ke, Y.; Liu, Y.; Chhabra, R.; Yan, H. *Nat. Nanotechnol.* **2008**, *3*, 418.
(21) (a) Cohen, J. D.; Sadowski, J. P.; Dervan, P. B. *Angew. Chem., Int. Ed.* **2007**, *46*, 7956. (b) Cohen, J. D.; Sadowski, J. P.; Dervan, P. B. *J. Am. Chem. Soc.* **2008**, *130*, 402.
(22) Garibotti, A. V.; Knudsen, S. M.; Ellington, A. D.; Seeman, N. C. *Nano Lett.* **2006**, *6*, 1505.
(23) (a) Wilner, O. I.; Weizmann, Y.; Gill, R.; Lioubashevski, O.; Freeman, R.; Willner, I. *Nat. Nanotechnol.* **2009**, *4*, 249. (b) Wilner, O. I.; Shimron, S.; Weizmann, Y.; Wang, Z.-G.; Willner, I. *Nano Lett.* **2009**, *9*, 2040.
(24) (a) Kuzuya, A.; Kimura, M.; Numajiri, K.; Koshi, N.; Ohnishi, T.; Okada, F.; Komiyama, M. *ChemBioChem* **2009**, *10*, 1811. (b) Numajiri, K.; Yamazaki, T.; Kimura, M.; Kuzuya, A.; Komiyama, M. *J. Am. Chem. Soc.* **2010**, *132*, 9937.
(25) (a) Endo, M.; Katsuda, Y.; Hidaka, K.; Sugiyama, H. *J. Am. Chem. Soc.* **2010**, *132*, 1592. (b) Endo, M.; Katsuda, Y.; Hidaka, K.; Sugiyama, H. *Angew. Chem., Int. Ed.* **2010**, *49*, 9412.
(26) (a) Niemeyer, C. M. *Angew. Chem., Int. Ed.* **2010**, *49*, 1200. (b) Saccà, B.; Meyer, R.; Erkelenz, M.; Kiko, K.; Arndt, A.; Schroeder, H.; Rabe, K. S.; Niemeyer, C. M. *Angew. Chem., Int. Ed.* **2010**, *49*, 9378.
(27) Shen, W.; Zhong, H.; Neff, D.; Norton, M. L. *J. Am. Chem. Soc.* **2009**, *131*, 6660.
(28) Stephanopoulos, N.; Liu, M.; Tong, G. J.; Li, Z.; Liu, Y.; Yan, H.; Francis, M. B. *Nano Lett.* **2010**, *10*, 2714.
(29) (a) Voigt, N. V.; Tørring, T.; Rotaru, A.; Jacobsen, M. F.; Ravnsbæk, J. B.; Subramani, R.; Mamdouh, W.; Kjems, J.; Mokhir, A.; Besenbacher, F.; Gothelf, K. V. *Nat. Nanotech.* **2010**, *5*, 200. (b) Liu, H.; Tørring, T.; Dong, M.; Rosen, C. B.; Besenbacher, F.; Gothelf, K. V. *J. Am. Chem. Soc.* **2010**, *132*, 18054.
(30) (a) Schwartz, E.; Gac, S. L.; Cornelissen, J. J. L. M.; Nolte, R. J. M.; Rowan, A. E. *Chem. Soc. Rev.* **2010**, *39*, 1576. (b) Su, W.; Schuster, M.; Bagshaw, C. R.; Rant, U.; Burley, G. A. *Angew. Chem., Int. Ed.* **2011**, *50*, 2712. (c) Stein, I. H.; Steinhauer, C.; Tinnefeld, P. *J. Am. Chem. Soc.* **2011**, *133* (12), 4193–4195.
(31) Varghese, R.; Wagenknecht, H.-A. *Chem.—Eur. J.* **2009**, *15*, 9307.
(32) The chemical structure of **AF** was taken from Chiuman, W.; Li, Y. *Nucleic Acids Res.* **2007**, *35*, 401.
(33) Wang, R.; Liu, W.; Seeman, N. C. *Chem. Biol.* **2009**, *16*, 862.
(34) Ranjit, S.; Gurunathan, K.; Levitus, M. *J. Phys. Chem. B* **2009**, *113*, 7861.
(35) Iqbal, A.; Arslan, S.; Okumus, B.; Wilson, T. J.; Giraud, G.; Norman, D. G.; Ha, T.; Lilley, D. M. *Proc. Natl. Acad. Sci. U.S.A.* **2008**, *105*, 11176.
(36) Lakowicz, J. R. *Principles of Fluorescence Spectroscopy*, 3rd ed.; Springer: New York, 2006.